Machine learning based study of microchannel plate detector configurations for future NICA experiments

Authors: Galaktionov K.A., Roudnev V.A., Valiev F.F.
Presentation: Galaktionov K.A.

St. Petersburg University

MPD Cross-PWG Meeting, 18 October 2022
https://indico.jinr.ru/event/3279/

Microchannel plate detectors

Some features of these detectors:

- Variability in size
- Registration of charged particles
- Time of flight resolution $\approx$ 50 - 100 ps

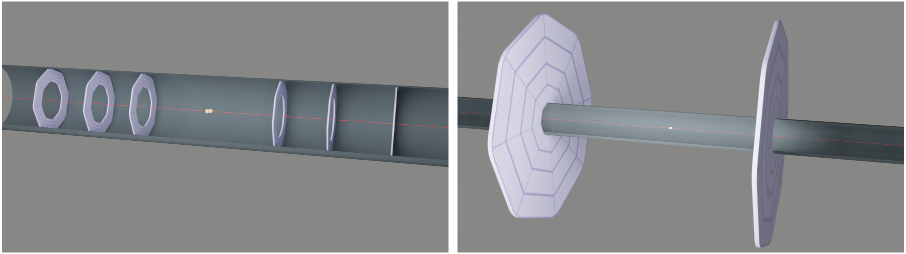

Fig. 1 Scheme of modeled detector configurations (not to scale). (left) - inside vacuum beam-pipe, three pairs of small rings (d = 3 cm, D = 5 cm), (right) - outside the beam-pipe in thin-wall vacuum chambers, one pair of big rings (d = 5 cm, D = 50 cm).

Research method

1. The QGSM model of gold nuclei collisions ($\sqrt{(s)} = 11$GeV/nucleon) is used as a source data.
2. Spacial and temporal data for the detector hits is generated according to the detector configuration.
3. The detector data is used for the neural network training.

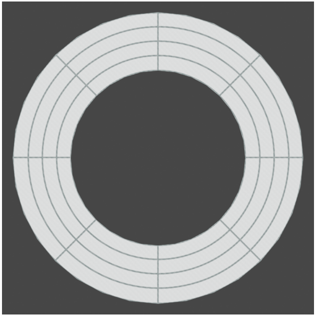

Fig. 2 Example of partitioning the detector into cells by radius and angle

Artificial neural networks (ANN)

ANN - an example of supervised learning.
Formula describing a dense layer of a neural network.

$$y = \theta(x * A^T + b) \tag{1}$$

Formula describing a convolutional layer of a neural network.

$$out(N_i, C_{out_j}) = \theta(bias(C_{out_j}) + \sum_{k=0}^{C_{in}-1} weight(C_{out_j}, k) \star input(N_i, k)) \tag{2}$$

Where: y, out - outputs of layer; $x, input$ - inputs of layer; A^T - transpose of a matrix of weights; $weight$ - convolution kernel; b, bias - biases of layer, $\theta(x)$ - activation function.

One pair of big rings. Event features

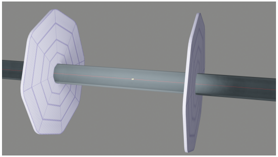

Fig. 3 Scheme of the configuration

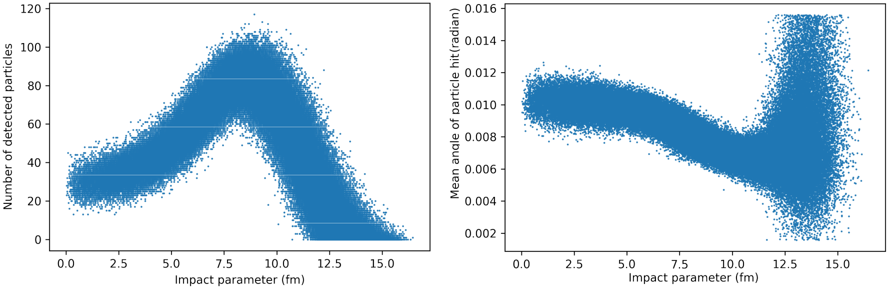

Fig. 4 Event features dependence on the impact parameter of an event. (left) - number of registered particles, (right) - mean angle of particle (first moment of distribution)

One pair of big rings. Regression results

To make more realistic situation coordinate of the collision was taken from the normal distribution (mean = 0 cm, standard deviation = 15 cm) (results are in the right plot)

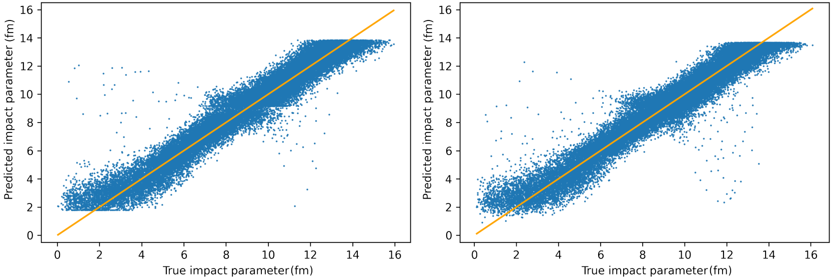

Fig. 5 Dependence of the evaluated impact parameter on the true value. (left) - collisions in the same point, $\sigma = 0.78$fm, (right) - collisions with distributed coordinate, $\sigma = 0.80$fm

One pair of big rings. Classification results

The goal is to divide all events into two classes. Class 1 - impact parameter below threshold, Class 2 - above.

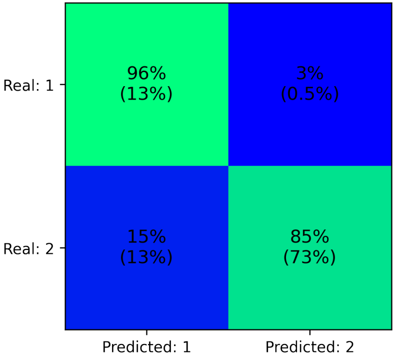

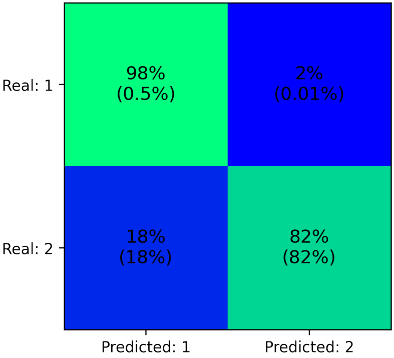

Fig. 6 Confusion matrices: (left) - threshold = 5 fm. Overall accuracy reaches 86 %, (right) - threshold = 1 fm. Overall accuracy reaches 82 %

One pair of big rings. Classification results, distributed coordinate

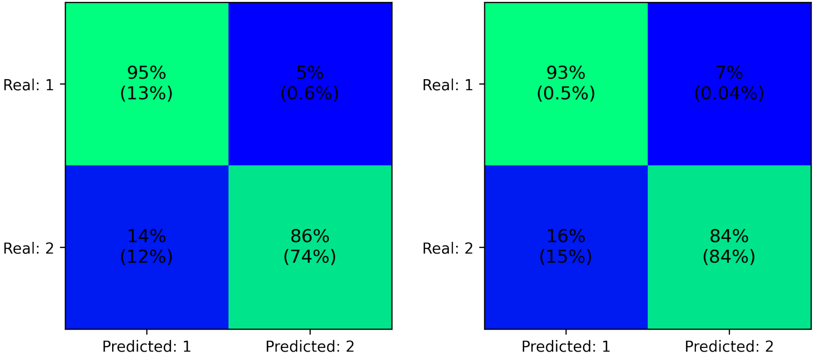

Fig. 7 Confusion matrices: (left) - threshold = 5 fm. Overall accuracy reaches 87 %, (right) - threshold = 1 fm. Overall accuracy reaches 84 %

One pair of big circles. Event features

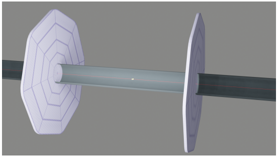

Fig. 8 Scheme of the configuration

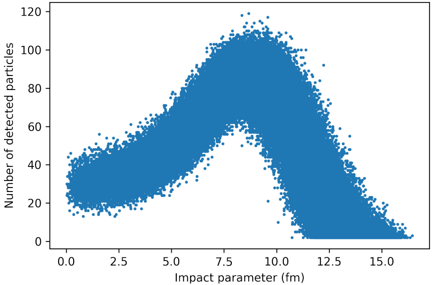

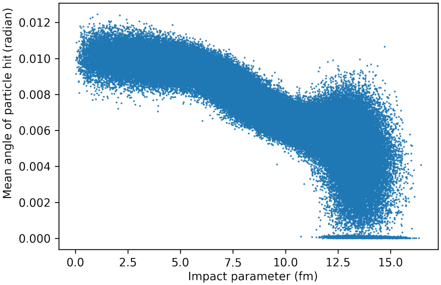

Fig. 9 Event features dependence on the impact parameter of an event. (left) - number of registered particles, (right) - mean angle of particle (first moment of distribution)

One pair of big circles. Classification results

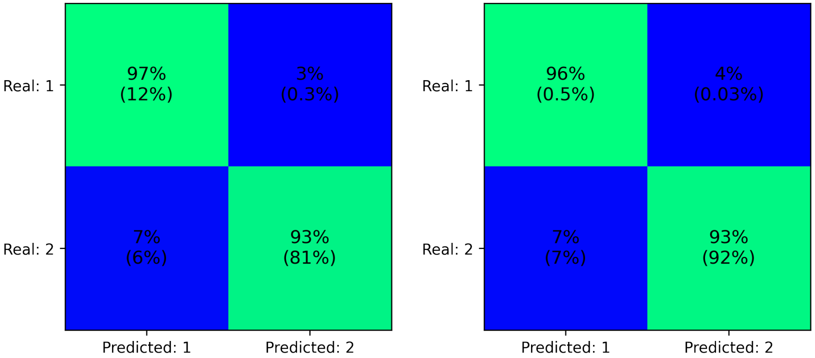

Fig. 10 Confusion matrices: (left) - threshold = 5 fm. Overall accuracy reaches 93 %, (right) - threshold = 1 fm. Overall accuracy reaches 92 %

Three pairs of small rings. Event features

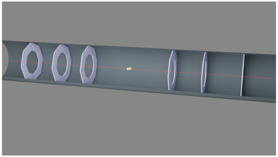

Fig. 11 Scheme of the configuration

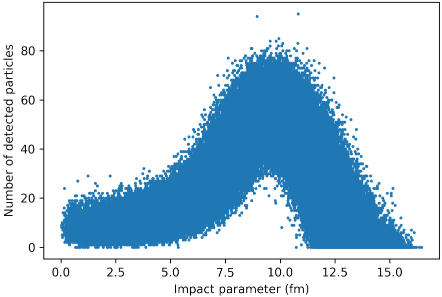

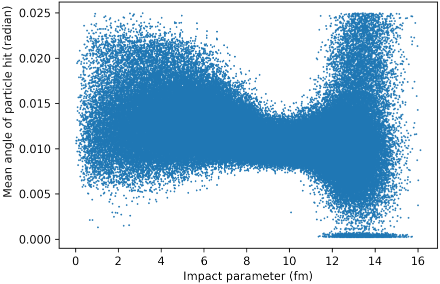

Fig. 12 Event features dependence on the impact parameter of an event. (left) - number of registered particles, (right) - mean angle of particle (first moment of distribution)

Three pairs of small rings. Time of flight

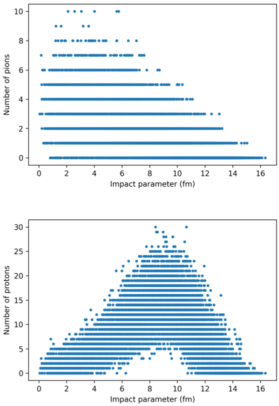

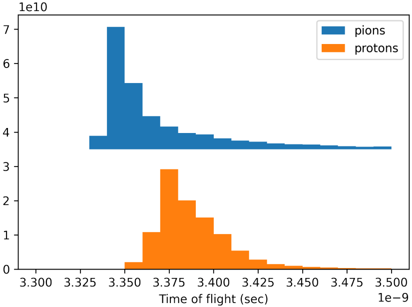

$$\nu = \frac{1}{t - t_{0i}} \tag{3}$$

Fig. 13 (left) - dependence of number of registered pions and protons (most part of the particles) on the impact parameter of an event (right) - pions and protons time-of-flight distribution and transformation formula, where t - time-of-flight, t_{0i} - average time of flight of pions on i-th detector

Three pairs of small rings. Regression results

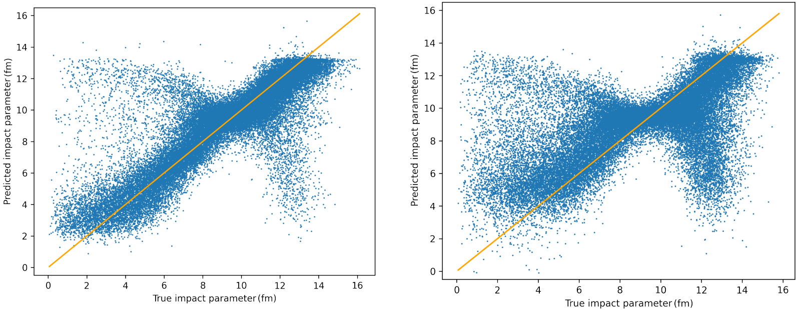

Fig. 14 Dependence of the evaluated impact parameter on the true value. (left) - collisions in the same point, $\sigma = 1.7$fm, (right) - collisions with distributed coordinate, $\sigma = 2.4$fm

Three pairs of small rings. Classification results

The goal is to divide all events into two classes. Class 1 - impact parameter below threshold, Class 2 - above.

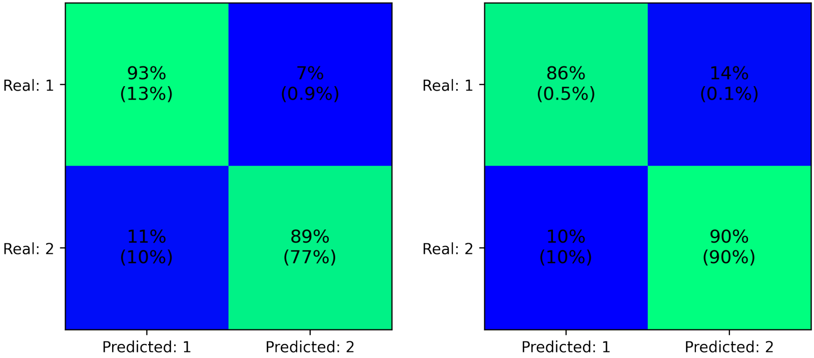

Fig. 15 Confusion matrices: (left) - threshold = 5 fm. Overall accuracy reaches 89 %, (right) - threshold = 1 fm. Overall accuracy reaches 90 %

Conclusion

Advantages of big detectors geometry:

- Usage of only statistical data
- Sustainable to the distribution of the collision coordinate
- Small neural network

Advantages of small detectors geometry:

- Cheaper to make
- Less data preprocessing
- Occupy less space

Overall comparison table

Detector type	Small rings detector	Big rings detector
Regression result (σ fm)	1.7	0.78
Regression (var. coord.) (σ fm)	2.4	0.80
5 fm classification, true positive	93.1 %	96.6 %
5 fm classification, true negative	88.6 %	84.9 %
1 fm classification, true positive	86.4 %	97.6 %
1 fm classification, true negative	90.1 %	82.0 %

Computational resources

Evaluation was performed by calculating the amount of floating point multiplications needed for the work of algorithm.

Big detectors geometry:

- 300 - 400 floating point multiplications
- Preprocessing: number of particles and mean angle
- 2 x 352 cells

Small detectors geometry:

- 10000 - 80000 floating point multiplications
- Preprocessing: time-of-flight evaluation
- 6 x 32 cells

All values are approximate and require fine tuning.